Weak-valued correlation functions: Insights and precise readout strategies

Yuan Feng [ORCID],[1,*] Xi Chen [ORCID],[2,3,†] and Yongcheng Ding [ORCID][2,‡]

[1]*Blackett Laboratory, Imperial College London, Prince Consort Road, London SW7 2AZ, United Kingdom*
[2]*Department of Physical Chemistry, University of the Basque Country UPV/EHU, Apartado 644, 48080 Bilbao, Spain*
[3]*EHU Quantum Center, University of the Basque Country UPV/EHU, 48940 Leioa, Spain*

The correlation function in quantum systems plays a vital role in decoding their properties and gaining insights into physical phenomena. Its interpretation corresponds to the propagation of particle excitations between space-time, similar in spirit to the idea of quantum weak measurement in terms of recording the system information by interaction. By defining weak-valued correlation function, we propose the basic insights and the universal methods for recording them on the apparatus through weak measurement. To demonstrate the feasibility of our approach, we perform numerical experiments of perturbed quantum harmonic oscillators, addressing the intricate interplay between the coupling strength and the number of ensemble copies. Additionally, we extend our protocol to the domain of quantum field theory, where joint weak values encode crucial information about the correlation function. Hopefully, this comprehensive investigation can advance our understanding of the fundamental nature of the correlation function and weak measurement in quantum theories.

I. INTRODUCTION

The correlation function is an indispensable aspect of quantum theory that furnishes a comprehensive characterization of the properties of quantum systems [1]. By unifying essential concepts, it serves as a powerful tool for investigating various quantities in quantum field theory, including scattering amplitudes, transition probabilities, and vertex amplitudes. Also, by employing Wick's trick, the correlation function provides insights into statistical behaviors in many-body physics [2]. The physical interpretation of the n-point correlator $\langle\Omega|\mathcal{T}[\hat{\phi}(\mathbf{x}_1)\cdots\hat{\phi}(\mathbf{x}_n)]|\Omega\rangle/\langle\Omega|\Omega\rangle$ corresponds to information extraction from the system with probing particles excitations. It is indeed the amplitude of a system preserving its ground state after (anti)particle excitations at space-times $(\mathbf{x}_1, \ldots, \mathbf{x}_n)$. Those excited particles could be viewed as probing particles or apparatuses due their weak nature compared to the whole system. Besides the more conventional correlator, the out-of-time correlator has also proven valuable in exploring engaging phenomena such as quantum chaos and information scrambling, which remain active frontiers of research [3–6].

Meanwhile, recent developments in quantum information allow us to retrieve the information of a quantum system through interacting with the apparatus. In particular, weak measurement of the Aharonov-Albert-Vaidman (AAV) formalism [7] has emerged as a novel way of recording the information on the pointer while weakly disturbing the system, an idea similar to the interpretation of the correlation function mentioned above. Weak measurements have led to a range of cutting-edge experiment proposals [8,9] and advancements [10,11], using this technique. These experiments include the recording of physical quantities [12–14], quantum tomography [15,16], quantum steering [17–19], and transition detection [20,21].

This similarity of extracting information via weak interaction motivates us to consider the weak-valued correlation function as the outcome of a weak measurement. Interestingly, this perspective is also supported by the Gell-Mann–Low theorem, as well as the two-state vector formalism. In the calculation of the correlation function, it is customary to invoke the Gell-Mann–Low theorem [22] before embarking on Feynman diagram calculations. This theorem allows one to recast the n-point correlator $\langle\Omega|\mathcal{T}[\hat{\phi}(\mathbf{x}_1)\cdots\hat{\phi}(\mathbf{x}_n)]|\Omega\rangle/\langle\Omega|\Omega\rangle$ as a sum of connected diagrams with n external lines. The physical interpretation of it entails the evolution of two vacuum states $\langle 0||0\rangle$ from the infinite past and future to the state $\langle\Omega||\Omega\rangle$ in the present. If we adopt a time-symmetric perspective, the two-state vector formalism (TSVF) [23,24] could be introduced as an alternative to the Gell-Mann–Low theorem. Without requiring adiabaticity, the TSVF allows for an arbitrary Hamiltonian to guide the evolution of eigenstates towards the preselection or postselection state, offering us the weak-valued interpretation of the correlation function [25].[1]

---

*yuan.feng0630@gmail.com
†chenxi1979cn@gmail.com
‡jonzen.ding@gmail.com

---

[1]Recently, we became aware of Ref. [25], which aims at showing a new interpretation of the weak value, whereas in the present work we focus on the weak-valued correlation function.

In this article we define the weak-valued correlation function using the standard AAV formalism, where the correlation function is viewed as the result of weak measurement. In Sec. II we propose the general ideas and universal schemes for recording the correlation function on the apparatus through weak measurement. In Sec. III we start with the perturbed quantum harmonic oscillator as the minimal example to exemplify our scheme. By measuring eigenvalues, we estimate the final apparatus state, yielding complex readouts [26]. Our findings reveal the trade-off between measurement strength and the number of experimental copies. This trade-off determines an optimal coupling coefficient, allowing the closest estimation of weak values with limited experimental copies. In Sec. IV we further extend our analysis to quantum field theory utilizing the framework proposed by Dressel *et al.* [27], which presents an alternative paradigm for implementing weak measurement. In Sec. V we analyze the pivotal role of the Gell-Mann–Low theorem and TSVF in the weak-valued correlation function as part of the motivation of our work. We also discuss the experimental realization and further investigation of correlators and quantum foundations. We briefly summarize in Sec. VI.

II. WEAK-VALUED CORRELATION FUNCTION

The basic idea of the weak-valued correlation function (WVCF) is to construct the space-time excitation of the correlation function through weak measurement. This could be realized through measuring the excitation operator of the system defined by

$$\hat{G} = \mathcal{T}[\hat{\phi}(\mathbf{x}_1) \cdots \hat{\phi}(\mathbf{x}_n)] \tag{1}$$

under pre- and postselection of the system into the ground state $|\Omega\rangle$. The scheme of the AAV-type weak measurement giving the WVCF is as follows. We begin by preparing the system's quantum state in the preselection state $|\Omega\rangle$ and the apparatus in an arbitrary state $|\phi\rangle$, which combine together into a separable state $|\Omega\rangle \otimes |\phi\rangle$. Then we couple the system and apparatus using an impulsive interaction

$$H_{\text{int}} = g\delta(t - t_0)\hat{G} \otimes \hat{A}, \tag{2}$$

where $\hat{A}$ is the Hermitian operator of the apparatus used for coupling. Finally, after postselection $|\Omega\rangle$ on the system, the whole state evolves into $\langle\Omega|\Omega\rangle(|\Omega\rangle \otimes e^{-igG_w\hat{A}}|\phi\rangle)$, in the weak-coupling regime $g \to 0$. Here G_w is usually called a weak value for $\hat{G}$ and different space-time $(\mathbf{x}_1, \ldots, \mathbf{x}_n)$ gives different $\hat{G}$ and thus different values of G_w. Thus, we define $G_w(\mathbf{x}_1, \ldots, \mathbf{x}_n)$ as the WVCF, which converges to the true value of the correlation function in the limit of $g \to 0$:

$$G_w(\mathbf{x}_1, \ldots, \mathbf{x}_n) \to \frac{\langle\Omega|\mathcal{T}[\hat{\phi}(\mathbf{x}_1) \cdots \hat{\phi}(\mathbf{x}_n)]|\Omega\rangle}{\langle\Omega|\Omega\rangle}, \quad g \to 0. \tag{3}$$

To precisely read out the WVCF recorded in the final state of the apparatus, we resort to the average value of any operator $\hat{M}$ of the apparatus in the final state (derivation details are in Appendix C)

$$\langle\hat{M}\rangle_f \simeq \langle\hat{M}\rangle_i + ig\langle\hat{A}\hat{M} - \hat{M}\hat{A}\rangle_i \text{Re}G_w$$
$$+ g(\langle\hat{A}\hat{M} + \hat{M}\hat{A}\rangle_i - 2\langle\hat{M}\rangle_i\langle\hat{A}\rangle_i)\text{Im}G_w, \tag{4}$$

where $\langle\cdots\rangle_i$ corresponds to the average over the initial state of the apparatus $|\phi\rangle$ and $\langle\cdots\rangle_f$ corresponds to the average over the final state of the apparatus $e^{-igG_w\hat{A}}|\phi\rangle$. Here Eq. (4) corresponds to a set of equations of two unknown variables $\text{Re}G_w$ and $\text{Im}G_w$, the solution of which gives us G_w.

Note that there are other well-known definitions of weak measurement, e.g., the continuous-in-time positive-operator-valued measure [28,29]. However, the weak measurement in this paper refers to only the standard AAV formalism that consists of a preselection on the system, system-apparatus coupling, and a postselection on the system, accumulating a weak value of the apparatus wave function.

Furthermore, our definition of the WVCF and the weak measurement scheme could be directly generalized to quantum field systems by considering the system and apparatus as two separate degrees of freedom of a quantum field and by considering the pre- and postselected states as the boundary conditions of the quantum field [27]. To define the WVCF, we need to perform the polar decomposition $\hat{G} = \hat{U}\hat{R}$ (see Sec. IV for an explanation), where $\hat{U}$ is a unitary operator and $\hat{R}$ is a Hermitian positive-semidefinite operator [30]. This time we measure the Hermitian part $\hat{R}$ of the excitation operator

$$H_{\text{int}} = g\delta(t - t_0)\hat{R} \otimes \hat{A} \tag{5}$$

under the preselection $|I\rangle = |\Omega\rangle \otimes |I_a\rangle$ and postselection $|F\rangle = |\Theta\rangle \otimes |F_a\rangle$, where $|\Theta\rangle = \hat{U}^\dagger|\Omega\rangle$. According to the quantum action principle [31], the variation of detection probability is given by

$$\delta \ln \text{p} = 2\delta g(\text{Re}R_w\text{Im}A_w + \text{Im}R_w\text{Re}A_w), \tag{6}$$

where $p = |\langle F| \exp(-i \int \hat{H}_{\text{int}}dt)|I\rangle|^2$ is the detection probability of the quantum field and $A_w = \langle F_a|\hat{A}|I_a\rangle/\langle F_a|I_a\rangle$ is the weak value of $\hat{A}$. To extract the weak value R_w, we perform measurements on the left-hand side of Eq. (6), utilizing suitable preselection $|I_a\rangle$ and postselection $|F_a\rangle$ states to solve the corresponding linear equations. The solution of Eq. (6) gives us $R_w \to \frac{\langle\Theta|\hat{R}|\Omega\rangle}{\langle\Theta|\Omega\rangle}$ when $\delta g \to 0$. We call R_w a weak-valued Hermitian function. Accordingly, we define the WVCF in the quantum field as

$$G_w = R_w\frac{\langle\Theta|\Omega\rangle}{\langle\Omega|\Omega\rangle} \to \frac{\langle\Omega|\mathcal{T}[\hat{\phi}(\mathbf{x}_1) \cdots \hat{\phi}(\mathbf{x}_n)]|\Omega\rangle}{\langle\Omega|\Omega\rangle}, \quad \delta g \to 0. \tag{7}$$

The details of readout strategies in quantum field theory will be discussed in Sec. IV.

In this work we focus on this type of measurement and refrain from discussing the detailed implementation on a specific quantum platform at this stage. Although the operator being measured may be a product of local operators, the response obtained through weak measurements aligns with the established theory of a weak value [32]. Moreover, the theory remains valid even in cases where nonlocal interactions are necessary for certain tasks, enabling experimental devices to realize joint weak values [33].

III. SIMPLEST CASE: PERTURBED QUANTUM HARMONIC OSCILLATOR

Next we exemplify our proposal in quantum mechanics, by considering the perturbed quantum harmonic oscillator (PQHO). The Hamiltonian reads $H = p^2/2m + m\omega^2 x^2/2 + \lambda x^4$, where the anharmonic perturbation λx^4 is treated as the self-interaction term. Without loss of generality, we define the excitation operator at an arbitrary time $t \geqslant 0$,

$$\hat{G} = x(t)x(0) = e^{iHt}xe^{-iHt}x; \tag{8}$$

its weak values correspond to the correlation function of the PQHO.

To perform the weak measurement, we employ a qubit as the apparatus to record the weak value. We prepare the separable initial state $|\Omega\rangle \otimes [\cos(\frac{\theta_0}{2})|\uparrow\rangle + \sin(\frac{\theta_0}{2})e^{i\varphi}|\downarrow\rangle]$, where $|\uparrow\rangle$ and $|\downarrow\rangle$ are the eigenbasis of $\hat{\sigma}_z$. Then we couple the excitation operator of the system and the spin-y operator of the apparatus using an impulsive interaction $H_{\text{int}} = g\delta(t - t_0)\hat{G} \otimes \hat{\sigma}_y$, which entangles the quantum states of the system and apparatus. After the postselection $|\Omega\rangle$, the WVCF accumulates on the final state of the apparatus, given by $e^{-igG_w\hat{\sigma}_y}|\phi\rangle$. It is worth noting that in the limit of $g \to 0$, they converge to the true values.

The physical interpretation of the WVCF corresponds to a rotation through a small angle $\theta - \theta_0 = 2gG_w$ around the Y axis, assuming G_w is real. In the case of a complex weak value $G_w = \text{Re}G_w + i\,\text{Im}G_w$ [26], we need to analyze the effect of the nonunitary operator $e^{-igG_w\hat{\sigma}_y}$ on the apparatus, to retrieve the value of correlator at an arbitrary time. In the weak-coupling regime, the expectation values of the qubit in different directions satisfy the equations (see Appendix C for details)

$$\langle\hat{\sigma}_y\rangle_f \simeq \langle\hat{\sigma}_y\rangle_i + 2g(1 - \langle\hat{\sigma}_y\rangle_i^2)\text{Im}G_w,$$

$$\langle\hat{\sigma}_x\rangle_f \simeq \langle\hat{\sigma}_x\rangle_i + 2g\langle\hat{\sigma}_z\rangle_i\text{Re}G_w - 2g\langle\hat{\sigma}_x\rangle_i\langle\hat{\sigma}_y\rangle_i\text{Im}G_w, \tag{9}$$

$$\langle\hat{\sigma}_z\rangle_f \simeq \langle\hat{\sigma}_z\rangle_i - 2g\langle\hat{\sigma}_x\rangle_i\text{Re}G_w - 2g\langle\hat{\sigma}_z\rangle_i\langle\hat{\sigma}_y\rangle_i\text{Im}G_w.$$

By measuring the expectation values of the spin components, we can access the value of G_w. With the estimations of $\langle\hat{\sigma}_y\rangle_f$ and $\langle\hat{\sigma}_x\rangle_f$, we estimate the WVCF as

$$\text{Im}G_w = \frac{\langle\hat{\sigma}_y\rangle_f - \langle\hat{\sigma}_y\rangle_i}{2g(1 - \langle\hat{\sigma}_y\rangle_i^2)},$$

$$\text{Re}G_w = \frac{\langle\hat{\sigma}_x\rangle_i\langle\hat{\sigma}_y\rangle_i}{\langle\hat{\sigma}_z\rangle_i}\text{Im}G_w + \frac{\langle\hat{\sigma}_x\rangle_f - \langle\hat{\sigma}_x\rangle_i}{2g\langle\hat{\sigma}_z\rangle_i}. \tag{10}$$

Figure 1 provides valuable insight into the behavior of our protocol in the PQHO model, highlighting the importance of operating within the weak-coupling regime to ensure accurate readout of the WVCF. The readout of our protocol is calculated through numerical simulations for different coupling strengths g according to Eq. (10). Here we approximate the perturbed ground state as $|\Omega\rangle \simeq |0\rangle + [(-3/2\sqrt{2})|2\rangle - (\sqrt{6}/8)|4\rangle]\lambda$ in the eigenbasis of the harmonic oscillator $|n\rangle$ and we express $\hat{G}$ in the basis of $|\Omega\rangle$ as a six-dimensional operator (see Appendixes A and B for details). We consider the calculated results under a six-dimensional cutoff as the true values.

By observing the expectation values $\langle\hat{\sigma}_x\rangle_f$ and $\langle\hat{\sigma}_y\rangle_f$ and solving Eqs. (9), which hold only in the weak-coupling
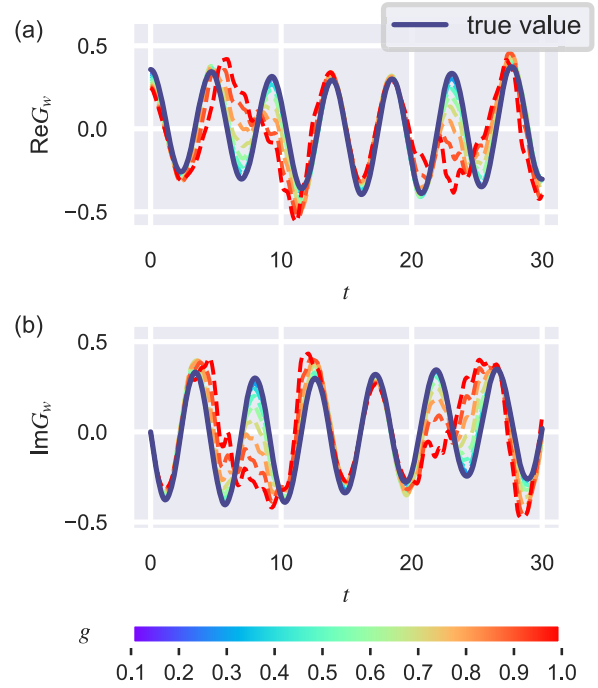

FIG. 1. Weak-valued correlation function determined from Eq. (10) for different measurement strengths g during the time $t \in [0, 30)$ plotted as a function of (a) the real part and (b) the imaginary part. The true values of the correlation function are represented by a dark solid line, while the weak values are depicted as a series of colored dotted lines.

regime, we retrieve the WVCF. Our simulations demonstrate that the readout deviates significantly from the true value at larger value of g, indicating the occurrence of the weak-to-strong transition [20]. In this regime, the higher-order terms in the expansion of the evolving operator $\exp(-ig\hat{G} \otimes \hat{\sigma}_y)$ introduce non-negligible effects on the apparatus. However, we establish the validity of our protocol by showing that the readouts at $g = 0.1$ exhibit good agreement with the true values, confirming the accuracy of our approach. We underscore the significance of adhering to the weak-coupling regime for reliable and precise readout of the WVCF.

It is important to note that the simulations presented in Fig. 1 are idealized, assuming perfect estimations of the expectation values $\langle\hat{\sigma}_i\rangle_f$, i.e., requiring infinite copies of the final state $e^{-igG_w\hat{\sigma}_y}|\phi\rangle$. In experimental implementations, however, the accuracy of our readout depends on both the coupling strength and the number of available copies. Let us consider that we have access to $2N$ copies of the final state in a single experiment, allowing us to perform N shots of measurement on the operators $\hat{\sigma}_x$ and $\hat{\sigma}_y$, respectively. By averaging the eigenvalues $\sigma_i = \pm 1$ as the measurement outcomes, we obtain the imperfect estimations of $\langle\hat{\sigma}_i\rangle_f$ as $\langle\hat{\sigma}_i\rangle_E = \sum_{i=1}^{N}\sigma_i$. The discrepancy between $\langle\hat{\sigma}_i\rangle_f$ and $\langle\hat{\sigma}_i\rangle_E$ is bounded by $|\langle\hat{\sigma}_i\rangle_f - \langle\hat{\sigma}_i\rangle_E| \leqslant \varepsilon(N, \delta)$, where $\varepsilon(N, \delta)$ represents the upper bound on the measurement-induced deviation with a probability of $1 - \delta$. Several explicit bounds can be used, such as the empirical Bernstein bound [34], which is applicable in various cases. Moreover, in practical scenarios, the optimal coupling strength is not necessarily the weakest possible. When the
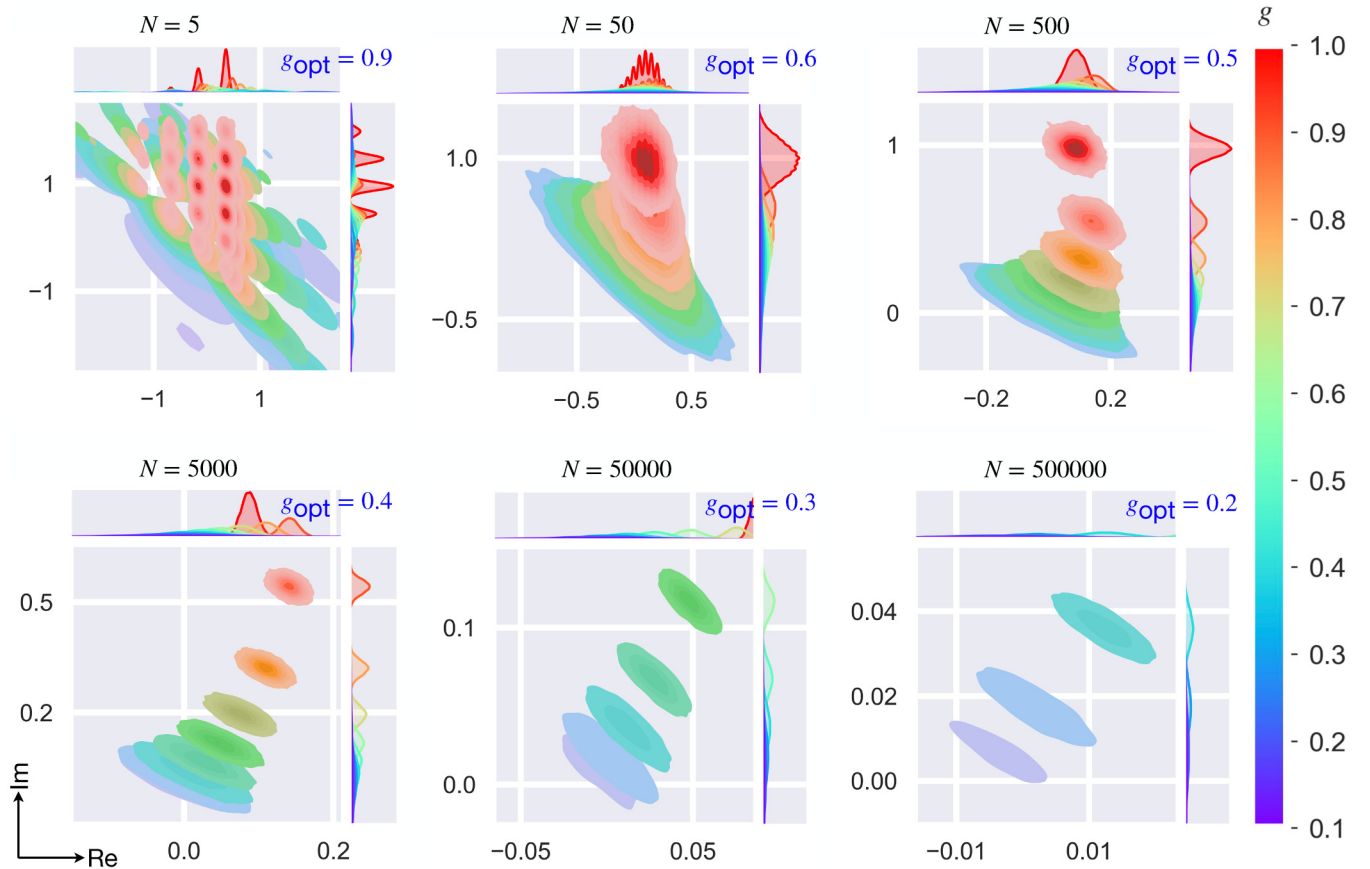
FIG. 2. Gaussian kernel density distribution of the relative radical vector $z_{RV} = (z_R - z_{TV})/|z_{TV}|$ on the complex plane, for various numbers of copies $2N$ and coupling strengths g. The marginal density distributions are shown at the top and on the right-hand sides sides, providing additional information about the distribution characteristics. In the top right corner of each panel we indicate the optimal value of the coupling strength g for each corresponding N.

signal-to-noise ratio decreases, extracting meaningful information from the apparatus becomes more challenging, leading to less precise retrieval of the correlator value with a limited number of copies N. Conversely, a stronger coupling enables a more accurate estimation of $\langle \hat{\sigma}_i \rangle_f$, albeit with a larger deviation between the weak value and the true value. Thus, a trade-off exists between the coupling strength g and the number of copies $2N$. Depending on specific criteria, one can select an appropriate coupling strength for a given number of copies, aiming to achieve a readout that sufficiently approaches the true values.

In this spirit, we designed a numerical experiment to retrieve the WVCF in the practical situation. The main results of this experiment simulation are shown in Fig. 2, where we analyze the distribution of the relative error radical vector $z_{RV} = (z_R - z_{TV})/|z_{TV}|$ on the complex plane. Here z_R is the readout of the weak value based on the estimations $\langle \hat{\sigma}_i \rangle_E$ and z_{TV} is the true value of the correlator. We vary the coupling strength from weak ($g = 0.1$) to strong ($g = 1$) with an interval of 0.1 and examine the variation trend in the distribution of the radical vector z_{RV} by increasing the number of copies $2N$. We observe that with increasing $2N$, the distribution changes from a multiple-peaklike shape to a Gaussian distribution on the complex plane. In the few-shot cases ($N = 5, 50$), the discrete nature of the values of possible readouts, resulting from the estimations $\langle \hat{\sigma}_i \rangle_E$, is blurred by performing Gaussian

interpolation before plotting them as dots for illustrative purposes. As N increases significantly, the readout values tend to converge to a continuum limit, approximating a complex normal distribution. To ensure reliable distributions, we perform $M = 10\,000$ individual simulations with specific settings of g_i and N_j to minimize statistical fluctuations. In terms of the trade-off, our objective is to identify the coupling strength that maximizes the likelihood of minimal deviation between the readout and the true value in a single experiment. After analyzing the raw data, we indicate the optimal coupling strength for each $N \in [1, 10\,000]$ in Fig 3 (for the methodology and additional information see Appendix D). This numerical experiment yields valuable insights into the behavior of our protocol, aiding in the determination of the appropriate coupling strength and number of copies for accurately reading the WVCF.

IV. EXTENSION TO QUANTUM FIELD THEORY: ϕ^4 THEORY

In the regime of weak interaction, the correlation function could be regarded as the weak value of field operator products under appropriate pre- and postselected boundary conditions [27]. Here we extend the concept of the WVCF to quantum field theory by considering the interaction between two separate degrees of freedom of the field under the

N	g_{opt}
[1, 3]	1
[4, 8]	0.9
[9, 14] ∪ {18}	0.8
[15, 43] \ {18}	0.7
[44, 202]	0.6
[203, 1043] \ {1036, 1038}	0.5
[1044, 8001] ∪ {1036, 1038, 8030} \ {7979}	0.4
[8002, 10 000] ∪ {7979}	0.3

FIG. 3. Detailed trade-off data of optimal $g \in G = \{0.1, 0.2, \ldots, 1\}$ for each $N \in [1, 10\,000]$.

pre- and post-space-time boundary conditions. We take ϕ^4 as an example to illustrate this extension. The Lagrangian density of the ϕ^4 theory is defined as $\mathcal{L} = \frac{1}{2}\partial^\mu \phi \partial_\mu \phi - \frac{1}{2}m^2 \phi^2 - \frac{\lambda}{4!}\phi^4$.

We consider the excitation operator at the origin and its polar decomposition:

$$\hat{G} = \mathcal{T}\phi(t, 0)\phi(0, 0) = \hat{U}\hat{R}. \tag{11}$$

Since the quantum action principle (6) only allows Hermitian operators, we need to separate the Hermitian part of the excitation operator using polar decomposition $\hat{G} = \hat{U}\hat{R}$ [30]. We denote the ground state by $|\Omega\rangle$ and after unitary transformation $|\Theta\rangle = \hat{U}^\dagger|\Omega\rangle$. We consider the orbital degree

of freedom of the local field as the system and the spin degree of freedom of the local field as the apparatus, which are two separate degrees of freedom of a local field. To carry out the weak measurement, we couple the Hermitian part of the excitation operator and the Pauli-x operator of the field $\hat{H}_{int} = g\delta(t - t_0)\hat{R} \otimes \hat{\sigma}_x$ under the initial $|I\rangle = |\Omega\rangle \otimes |I_a\rangle$ and final states of the field $|F\rangle = |\Theta\rangle \otimes |F_a\rangle$. By applying the quantum action principle [1,31], we have the joint weak value of the Hermitian variation of the quantum action $\delta\hat{S} = -\delta g\hat{R} \otimes \hat{\sigma}_x$, which encodes the amplitude $a = \langle F|\exp(-i \int \hat{H}_{int}dt)|I\rangle = \langle\Theta| \otimes \langle F_a|e^{-ig\hat{R}\otimes\hat{\sigma}_x}|\Omega\rangle \otimes |I_a\rangle$ as a weak value $S_w = \langle F|\delta\hat{S}|I\rangle/\langle F|I\rangle = -i\hbar\delta \ln a$, giving Eq. (6). To get R_w, we choose $|I_a\rangle_1 = |\uparrow\rangle$ and $|F_a\rangle_1 = 1/\sqrt{2}(|\uparrow\rangle + |\downarrow\rangle)$, and $|I_a\rangle_2 = 1/\sqrt{2}(i|\uparrow\rangle + |\downarrow\rangle)$ and $|F_a\rangle_2 = |\downarrow\rangle$ for convenience,

$$\text{Re}(R_w) = \delta \ln p_2/(2\delta g),$$
$$\text{Im}(R_w) = \delta \ln p_1/(2\delta g), \tag{12}$$

where $p = |a|^2$ is the detection probability and δg is the tunable coupling strength. We can retrieve the WVCF $G_w = R_w\langle\Theta|\Omega\rangle/\langle\Omega|\Omega\rangle$ by multiplying R_w with $\langle\Theta|\Omega\rangle/\langle\Omega|\Omega\rangle$, which interestingly coincides with the amplitude between the selection on the first degree of freedom of the local field.

To demonstrate the protocol, we simulate the weak-valued two-time correlation function of a ϕ^4 lattice field theory with $(1 + 1)$-dimensional space-time in Fig. 4. Based on the quantum action principle, it provides an alternative paradigm for weak measurement, differing from the standard AAV formalism. As an infinitesimal variation, this paradigm is closely related to the path-integral formalism and can be applied in quantum mechanics. (Refer to Appendix E for all simulation details.)
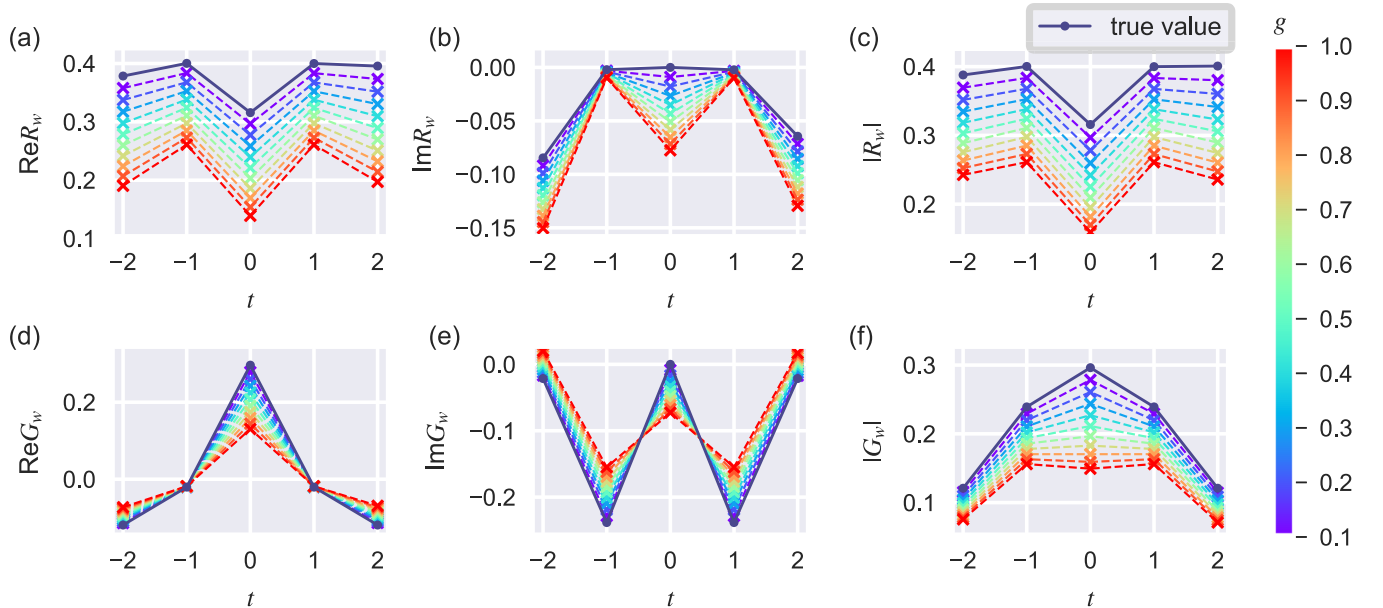

FIG. 4. Numerical simulations of a ϕ^4 lattice field theory. The weak-valued effective Hermitian function R_w of a ϕ^4 lattice field theory determined from Eq. (12) for different measurement strengths g during the time $t \in \{-2, -1, \ldots, 2\}$ is plotted in (a) the real part, (b) the imaginary part, and (c) the module. The corresponding weak-valued correlation function obtained from $G(t, 0) = R_w\langle\Theta|\Omega\rangle/\langle\Omega|\Omega\rangle$ is plotted in (d) the real part, (e) the imaginary part, and (f) the module. We plot the true values of the correlation function as dark dots, while weak values are plotted as colored crosses.

V. DISCUSSION AND OUTLOOK

After formulating the WVCF and its readout strategies in quantum mechanics and quantum field theory, we discuss the equivalence between the TSVF and the Gell-Mann–Low (GL) theorem in the interpretation of correlation functions. It also serves as the inspiration for this work. Following the GL theorem, we derive ground states $|\Omega^{\mp}\rangle = \lim_{\epsilon \to 0} U_{\epsilon I}(0, \mp\infty)|0\rangle / \langle 0|U_{\epsilon I}(0, \mp\infty)|0\rangle$ by adiabatically evolving the vacuum state $|0\rangle$ from infinite past or future to the present. Here $U_{\epsilon I}(0, \mp\infty)$ is the time-evolution operator corresponding to the Hamiltonian $H_{\epsilon}(t) = H_0 + e^{-\epsilon|t|}\lambda V$, which is known as the Møller operator [35]. Thus, we write the *n*-point correlation function of the corresponding system $G^{(n)}(\mathbf{x}_1, \ldots, \mathbf{x}_n) = \langle 0|\mathcal{T}[\hat{\phi}_I(\mathbf{x}_1) \cdots \hat{\phi}_I(\mathbf{x}_n)\mathcal{S}]|0\rangle / \langle 0|\mathcal{S}|0\rangle = \langle \Omega^+|\mathcal{T}[\hat{\phi}(\mathbf{x}_1) \cdots \hat{\phi}(\mathbf{x}_n)]|\Omega^-\rangle / \langle \Omega^+|\Omega^-\rangle$, satisfying the adiabatic criteria to preserve the ground state. Note that the GL theorem is not compulsory to derive the same expression. For example, we have an alternative way to arrive at the ground state from the vacuum state, departing from finite past t_1 and future t_2 to the preselected state $|\Omega^-\rangle = U(t_{\text{now}}, t_1)|0\rangle$ and postselected state $\langle \Omega^+| = \langle 0|U^{\dagger}(t_2, t_{\text{now}})$ at a certain time t_{now}. Accordingly, we can introduce an auxiliary potential in the total Hamiltonian to compensate for excitations or design a schedule for turning on the perturbation. Propagators $U(t_{\text{now}}, t_1)$ and $U^{\dagger}(t_2, t_{\text{now}})$ serve as shortcuts to adiabaticity [36,37], providing a more efficient way than the adiabatic evolution in the GL theorem. Thus, we derive the same expression of the correlation function, which can be understood as a weak value.

Considering the experimental implementation, one may turn to digital quantum simulation, a flexible method for exploring quantum dynamics of both quantum mechanics and quantum field theory [38,39]. This approach allows entanglement and selections with quantum circuits. Alternatively, one also has the standard technique in quantum field theory by introducing weak source currents linearly coupled to the field in the Lagrangian, perturbing the field evolution within local apparatuses. The joint averaged response of these apparatuses reveals the desired correlators, shedding light on the dynamics and properties of the investigated quantum field system.

Going beyond the examples in the work, a compelling application lies in reading out out-of time-order correlations, using weak measurement, where operators are non-time-ordered. Additionally, we can explore scattering matrix modulation with different pre- and postselections to study nonequilibrium physics and quantum nonlocality through propagators. Meanwhile, it is also compatible with the Keldysh formalism [40] that extends backward propagation in the calculation of the generalized correlation function, providing a systematic framework for investigating nonequilibrium systems [41–43].

VI. CONCLUSION

We have introduced the WVCF in a quantum system and quantum field as the result of weak measurement. We proposed a standard weak measurement of the AAV type to read out the WVCF of the PQHO. Our results reveal the interplay between the coupling strength and the number of copies in the readout. Furthermore, we extended our framework to quantum field theory, where correlator calculations are crucial. Finally, we redefined the Gell-Mann–Low theorem to develop a method for calculating the correlation function. By employing the TSVF to accelerate adiabatic evolution, we established an equivalent theory where the correlation function is interpreted as a weak value.

All codes and simulation data are available at [44].

APPENDIX A: GROUND STATE FROM THE GELL-MANN–LOW THEOREM

To calculate the ground state $|\Omega\rangle$ of the perturbed PQHO using the Gell-Mann–Low theorem, we consider the adiabatic Hamiltonian given by

$$H_{\epsilon}(t) = \frac{p^2}{2m} + \frac{1}{2}m\omega^2 x^2 + \lambda e^{-\epsilon|t|}x^4. \tag{A1}$$

We begin by focusing on the ground state $|\Omega^-\rangle$. Expanding the state in terms of a perturbation series, we express the target state as the ratio of two sets of infinite series

$$|\Omega^-\rangle = \lim_{\epsilon \to 0} \frac{U_{\epsilon I}(0, -\infty)|0\rangle}{\langle 0|U_{\epsilon I}(0, -\infty)|0\rangle}$$

$$= \lim_{\epsilon \to 0} \frac{\sum_{n=0}^{\infty} c_n \lambda^n}{\sum_{n=0}^{\infty} b_n \lambda^n} = \sum_{n=0}^{\infty} a_n \lambda^n, \tag{A2}$$

where $U_{\epsilon I}$ is the adiabatic time-evolution operator in the interacting picture. The series division on the right-hand side is implemented as

$$a_n = 1/b_0[c_n - a_0 b_n - \cdots - a_{n-1}b_1], \quad n = 0, 1, 2, \ldots.$$

Here a_n represents the coefficients of the perturbation series expansion of the ground state, which we aim to determine. The calculation involves solving a recursive equation to obtain the values of a_n. By following this procedure, we can determine the ground state of the PQHO Hamiltonian using the Gell-Mann–Low theorem.

Indeed, complex analysis reveals that the series representation $|\Omega^-\rangle = \sum_{n=0}^{\infty} a_n^{(\epsilon)}\lambda^n$ is a divergent series, with an asymptotic expansion only valid to the first order. On the complex plane, considering $|\Omega^-\rangle$ as a complex function of λ, it is nonanalytic everywhere except at the origin. This can be

understood by considering the case where $\lambda < 0$. In this scenario, there is no minimum energy for the potential, resulting in the nonexistence of the ground state $|\Omega^-\rangle$. Consequently, there is no circle of convergence outside the origin point.

The order of the asymptotic expansion is determined in the following way. In terms of the Dyson expansion, the time-evolution operator is written as

$$U_{\epsilon I}(t, t_0) = 1 + (-i) \int_{t_0}^{t} dt_1 H_{\epsilon I}(t_1)$$
$$+ (-i)^2 \int_{t_0}^{t} dt_1 \int_{t_0}^{t_1} dt_2 H_{\epsilon I}(t_1) H_{\epsilon I}(t_2) + \cdots,$$

where $H_{\epsilon I}(t) = \lambda e^{iH_0 t} e^{-\epsilon |t|} x^4 e^{-iH_0 t}$ is the adiabatic Hamiltonian in the interaction picture. Acting on $|0\rangle$ and inserting the identity operator $1 = \sum_n |n\rangle\langle n|$ leads to

$$U_{\epsilon I}(t, t_0)|0\rangle = |0\rangle + (-i)\lambda \sum_n \frac{\langle n|x^4|0\rangle}{in + \epsilon}|n\rangle$$
$$+ (-i)^2 \lambda^2 \sum_{n,m} \frac{\langle n|x^4|m\rangle\langle m|x^4|0\rangle}{(in + 2\epsilon)(im + \epsilon)}|n\rangle + \cdots,$$

where $|n\rangle$ is the eigenbasis of the harmonic oscillator satisfying $\hat{H}_0|n\rangle = E_n|0\rangle$ and $E_n = n + \frac{1}{2}$. The ground state could be derived by putting this into Eq. (A2) and calculating the series division:

$$|\Omega^-\rangle = \sum_n a_n \lambda^n = a_0 + a_1\lambda + a_2\lambda^2 + \cdots,$$

$$a_0 = \langle x|0\rangle,$$

$$a_1 = -\frac{3}{2\sqrt{2}}|2\rangle - \frac{\sqrt{6}}{8}|4\rangle,$$

$$a_2 = \frac{75}{8\sqrt{2}}|2\rangle + \frac{9\sqrt{6}}{4}|4\rangle + \frac{17}{16}\sqrt{5}|6\rangle + \frac{3\sqrt{70}}{64}|8\rangle. \quad \text{(A3)}$$

To find the optimal order for asymptotic expansion, we study the correlation function at $t = 0$: $G^{(2)}(0, 0) = \langle\Omega|x^2|\Omega\rangle/\langle\Omega|\Omega\rangle$. Our simulation result of solving the eigenequations gives 0.3700. Reserving Eq. (A3) to first order gives 0.3570, which is close to the simulation result. However, when reserved to second order, it becomes 0.8484, with more deviation. As expected, the higher the order is, the greater deviation we get. Likewise, we get $|\Omega^+\rangle$ in a similar way: $|\Omega^+\rangle = |\Omega^-\rangle = |\Omega\rangle$. As a result, first order is the optimal asymptotic series for $|\Omega\rangle$:

$$|\Omega\rangle \simeq |0\rangle + \left(-\frac{3}{2\sqrt{2}}|2\rangle - \frac{\sqrt{6}}{8}|4\rangle\right)\lambda. \quad \text{(A4)}$$

APPENDIX B: TRUNCATED EIGENBASIS OF THE HARMONIC OSCILLATOR

In order to address the challenge of infinite dimensionality in the calculation of the operator $\hat{A} = x(t)x(0) = e^{i\hat{H}t}xe^{-i\hat{H}t}x$, a truncation approach is employed. This approach involves selecting a cutoff energy level N_{cutoff} that ranges from a sufficiently large value down to zero. For the sake of better illustration, we simulate the eigenequations of the
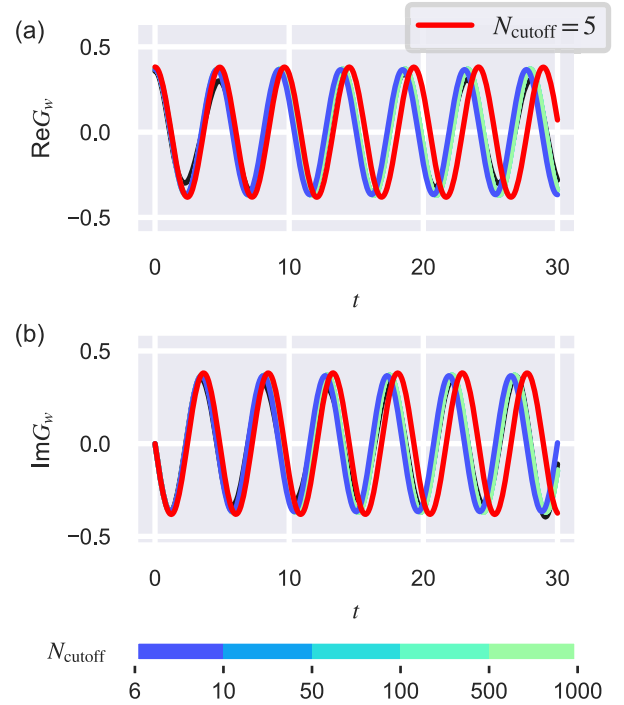

FIG. 5. Correlation function simulated for different cutoffs of the energy level N_{cutoff}. The colored curves are used to show numerical simulation of solving the eigenequations of the Hamiltonians for the N_{cutoff} at the bottom of (a) and (b). The black curve shows the result calculated from Eq. (A3) for a certain large enough cutoff energy level $N_{\text{cutoff}} = 1000$, which is almost covered by the colored curves at large N_{cutoff}. Here we utilize complementary colors to explicitly enhance the distinction between $N_{\text{cutoff}} = 5$ and $N_{\text{cutoff}} = 6$.

Hamiltonians under a sufficiently large cutoff of the energy level $N_{\text{cutoff}} = 1000$.

By expressing the operator $\hat{A}$ in terms of the eigenbasis of the harmonic oscillator, the cutoff energy level determines the range of energy levels considered in the calculation. As shown in Fig. 5, the behavior of the correlation function $G^{(2)}(t, 0)$ is observed as the cutoff energy level decreases. We note that as N_{cutoff} is reduced to $N_{\text{cutoff}} = 6$, the result from our calculation (A3) matches the simulation result and the value of $G^{(2)}(0, 0)$ remains constant at 0.356 972 59. However, a turning point is reached when N_{cutoff} reaches $N_{\text{cutoff}} = 5$, resulting in an obvious deviation from the simulation result and $G^{(2)}(0, 0) = 0.348 033 37$. This observation can be understood by considering that the calculated ground state is only relevant to the first five energy levels.

Based on these observations, a decision is made to choose $N_{\text{cutoff}} = 6$ as the truncated energy level for the calculation. This choice ensures that the relevant energy levels are included while controlling the computational complexity associated with the infinite-dimensional space.

APPENDIX C: COMPLEX WEAK VALUE THROUGH THE SPIN OF THE POINTER

For any complex weak value $G_w = a + bi$ measured through the interaction $\hat{G} \otimes \hat{A}$, any observable $\hat{M}$ of the
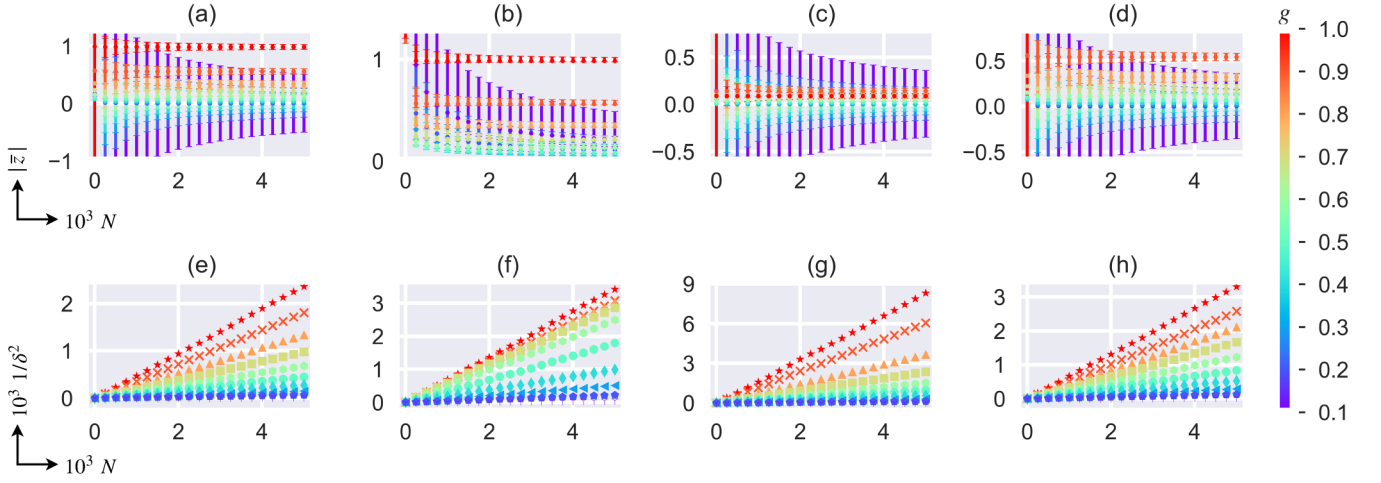
FIG. 6. Absolute mean values $|\bar{z}|$ are shown for $M = 10\,000$ sampling points of (a) complex value $z_{\mathrm{RV}} = (z_{\mathrm{R}} - z_{\mathrm{TV}})/|z_{\mathrm{TV}}|$, (b) module $|z_{\mathrm{RV}}| = |z_{\mathrm{R}} - z_{\mathrm{TV}}|/|z_{\mathrm{TV}}|$, (c) real part $\mathrm{Re}(z_{\mathrm{RV}}) = \mathrm{Re}(z_{\mathrm{R}} - z_{\mathrm{TV}})/|z_{\mathrm{TV}}|$, and (d) imaginary part $\mathrm{Im}(z_{\mathrm{RV}}) = \mathrm{Im}(z_{\mathrm{R}} - z_{\mathrm{TV}}))/|z_{\mathrm{TV}}|$. Error bars denote confidence intervals of 0.95. Uncertainty is plotted versus the number of copies $1/\delta^2 - N$ for $g \in G = \{0.1, 0.2, \ldots, 1\}$ over $M = 10\,000$ sampling points of (e) complex value $z_{\mathrm{RV}} = (z_{\mathrm{R}} - z_{\mathrm{TV}})/|z_{\mathrm{TV}}|$, (f) module $|z_{\mathrm{RV}}| = |z_{\mathrm{R}} - z_{\mathrm{TV}}|/|z_{\mathrm{TV}}|$, (g) real part $\mathrm{Re}(z_{\mathrm{RV}}) = \mathrm{Re}(z_{\mathrm{R}} - z_{\mathrm{TV}})/|z_{\mathrm{TV}}|$, and (h) imaginary part $\mathrm{Im}(z_{\mathrm{RV}}) = \mathrm{Im}(z_{\mathrm{R}} - z_{\mathrm{TV}})/|z_{\mathrm{TV}}|$. The relation $1/\delta^2 - N$ proves to be linear in all four cases.

apparatus satisfies

$$\langle \hat{M} \rangle_f = \langle \hat{M} \rangle_i + iga\langle \hat{A}\hat{M} - \hat{M}\hat{A} \rangle_i$$
$$+ gb(\langle \hat{A}\hat{M} + \hat{M}\hat{A} \rangle_i - 2\langle \hat{M} \rangle_i \langle \hat{A} \rangle_i), \quad \text{(C1)}$$

where we assume $\hat{A}$ is Hermitian. This equation is derived following the method in [26]. The initial and final states of the apparatus are $|\phi\rangle$ and $|\alpha\rangle = e^{-igG_w\hat{A}}|\phi\rangle \simeq (1 - igG_w\hat{A})|\phi\rangle$, where $|\phi\rangle$ is normalized but $|\alpha\rangle$ is not. The expectation of any operator $\hat{M}$ in the final state is, reserved to first order with the help of series division,

$$\langle \hat{M} \rangle_f = \frac{\langle \alpha|\hat{M}|\alpha \rangle}{\langle \alpha|\alpha \rangle}$$
$$\simeq \frac{\langle \phi|(\hat{M} - igG_w\hat{M}\hat{A} + ig\overline{G}_w\hat{A}\hat{M})|\phi \rangle}{\langle \phi|(1 - igG_w\hat{A} + ig\overline{G}_w\hat{A})|\phi \rangle}$$
$$= \frac{\langle \hat{M} \rangle + (ia\langle \hat{A}\hat{M} - \hat{M}\hat{A} \rangle_i + b\langle \hat{A}\hat{M} + \hat{M}\hat{A} \rangle_i)g}{1 + (2b\langle \hat{A} \rangle_i)g}$$
$$\simeq \langle \hat{M} \rangle_i + iga\langle \hat{A}\hat{M} - \hat{M}\hat{A} \rangle_i$$
$$+ gb\langle \hat{A}\hat{M} + \hat{M}\hat{A} \rangle_i - 2gb\langle \hat{M} \rangle_i \langle \hat{A} \rangle_i, \quad \text{(C2)}$$

which gives Eq. (C1). Letting $\hat{A} = \hat{\sigma}_y$ and putting spin components into M in Eq. (C1), we obtain Eq. (9).

APPENDIX D: NUMERICAL SIMULATION AND DETAILED TRADE-OFF DATA

In the numerical simulation, we focus on a specific time slice at $t = 5.1$ and consider a set of coupling constants $g \in G = \{0.1, 0.2, \ldots, 1\}$ for investigation. The number of copies N and number of repeated experiments M are both integers, with N ranging from 1 to 500 000 and M fixed at 10 000. Each repeated experiment is assigned a unique random seed ranging from 10 to 10 010.

For each experiment, we generate N random numbers following a uniform distribution over the interval $[0, 1)$. These random numbers are used to determine the measured values of $\langle \hat{\sigma}_x \rangle_f$ and $\langle \hat{\sigma}_y \rangle_f$. To calculate $\langle \hat{\sigma}_x \rangle_f$, we assign a value of -1 to random numbers that are smaller than the probability $|\langle \sigma_x = -1 | \alpha \rangle|^2/\langle \alpha|\alpha \rangle$ and $+1$ otherwise. Similarly, for $\langle \hat{\sigma}_y \rangle_f$, we use $|\langle \sigma_y = -1 | \alpha \rangle|^2/\langle \alpha|\alpha \rangle$ as the threshold to assign ± 1 to the random numbers.

To evaluate the accuracy of the measured results, we focus on the relative deviation from the true value, given by $z_{\mathrm{RV}} = (z_{\mathrm{R}} - z_{\mathrm{TV}})/|z_{\mathrm{TV}}|$. Utilizing Eq. (10), we obtain $M = 10\,000$ sampling points on the complex plane, denoted by $z_{\mathrm{RV}}(m; g, N)$, $m \in [0, M]$, for each combination of $g \in G$ and $N \in [1, 500\,000]$.

In the initial step, we study several important statistical quantities to gain a global understanding of the data set. Specifically, we calculate the mean values and variances for the complex value, module, real part, and imaginary part of z_{RV}. Figures 6(a)–6(d) summarize the results for $g \in G$ and $N \in [1, 5000]$. These panels clearly illustrate the trade-off between g and N as the transition from $N \sim 10$ to $N \sim 1000$ becomes apparent.

Additionally, we explore the uncertainty properties, paying particular attention to their dependence on N and g. Figures 6(e)–6(h) depict the variance versus the number of copies $1/\delta^2 - N$ for the complex value, module, real part, and imaginary part of z_{RV}. Horizontally, the perfect linearity in all four cases verifies our prediction that $\delta \sim 1/\sqrt{N}$. Vertically, the consistent ordering of $g \in G$ for a given N demonstrates that the uncertainty increases with smaller values of g.

Finally, we investigate the trade-off between g and N by determining the optimal value of $g \in G$ for different ranges of N. Figure 3 presents the optimal $g \in G$ for each $N \in [1, 10\,000]$. Our criterion for optimality is as follows. For a given N, we compare the distances to the true value $z_{\mathrm{RV}}(m; g_i, N) - z_{\mathrm{RV}}(m; g_j, N)$, $m \in [0, M]$, for any two $g_i, g_j \in G$. If the total number of cases where $z_{\mathrm{RV}}(m; g_i, N) - z_{\mathrm{RV}}(m; g_j, N) < 0$ is
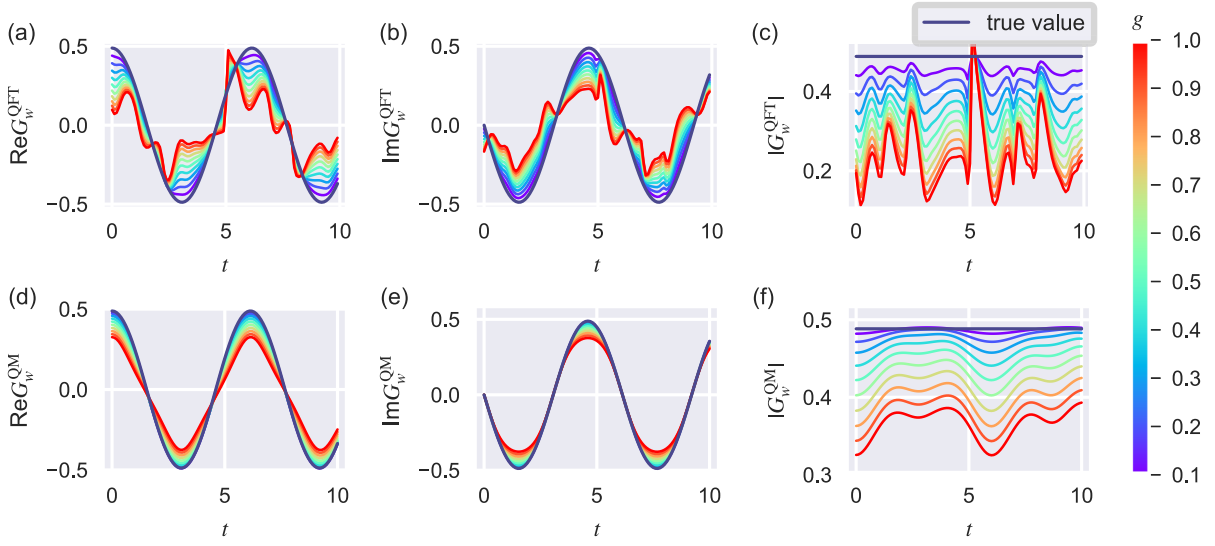
FIG. 7. Comparison of the one-lattice ϕ^4 theory with the PQHO weak-valued correlation function for different measurement strengths g during the continuous time $t \in [0, 30]$. Simulations of weak measurements in the QFT are shown for (a) the real part, (b) the imaginary part, and (c) the module and in QM for (d) the real part, (e) the imaginary part, and (f) the module.

greater than half of the total sampling $M = 10\,000$, we consider g_i to be dominant. The optimal value is the one that dominates over all other $g \in G$. In the case of a draw, we choose the one with the smallest value of g.

APPENDIX E: LATTICE SIMULATION OF THE ϕ^4 FIELD

We carry out the lattice simulation of the scalar ϕ^4 quantum field in a $(1 + 1) - d$ discretized Minkowski space-time, with periodic boundary conditions for both space and time. The space-time lattices are taken as integers given by $x^\mu = (t, x) = -l, -(l-1), \ldots, l-1, l$ with the lattice spacing $a = 1$. We set the initial configuration of ϕ^4 as

$$\phi_0(x) = \sqrt{L} \sum_p \frac{\Delta p}{2\pi} \frac{1}{\sqrt{2E_p}} (\hat{a}_p e^{-ipx} + \hat{a}_p^\dagger e^{ipx}), \quad \text{(E1)}$$

$$\pi_0(x) = \sqrt{L} \sum_p \frac{-i\Delta p}{2\pi} \sqrt{\frac{E_p}{2}} (\hat{a}_p e^{-ipx} - \hat{a}_p^\dagger e^{ipx}), \quad \text{(E2)}$$

where the energy momentum $E_p = (m^2 + p^2)^{1/2}$, $p = (2\pi/L)x$, the commutation relations $[\phi_0(x), \pi_0(y)] = i\delta_{xy}$ and $[\hat{a}_p, \hat{a}_{p'}^\dagger] = \delta_{pp'}$, and $L = 2l + 1$. The field operator of ϕ^4 could be obtained by switching on time evolution

$$\phi(t, x) = e^{i\hat{H}t} \phi(0, x) e^{-i\hat{H}t}, \quad \text{(E3)}$$

where $\hat{H} = 1/2 \sum_x \Delta x [\pi_0^2 + (\nabla\phi_0)^2 + m^2\phi_0^2 + \lambda/4!\phi_0^4]$.

In our numerical simulation, we consider $L = 5$, with a truncated Hilbert subspace $N_{\text{cutoff}} = 5$ for each individual lattice. The total dimension of the Fock space is $N = 5^5 = 3125$. The ground state $|\Omega\rangle$ is obtained by numerically solving the eigenequations of Hamiltonian. We perform the polar decomposition of the excita-

tion operator $\hat{G} = \mathcal{T}\phi(t, 0)\phi(0, 0)$ with the singular value decomposition method:

$$\hat{A} = \hat{u}\hat{s}\hat{v} = (\hat{u}\hat{v})(\hat{v}^\dagger sv) = \hat{U}\hat{R}. \quad \text{(E4)}$$

The variation of detection probability in Eq. (12) is simulated by the difference between the perturbed and the unperturbed $\delta p = p' - p = |\langle\Theta| \otimes \langle F_a| e^{-ig\hat{R}\otimes\hat{\sigma}_x} |\Omega\rangle \otimes |I_a\rangle|^2 - |\langle\Theta| \otimes \langle F_a|\Omega\rangle \otimes |I_a\rangle|^2$. Our simulation result of R_w is shown in Fig. 4. Similar to its quantum counterpart, the accuracy of the QFT weak measurement increases with small coupling g.

In order to explore the connection between weak measurements in quantum field theory (QFT) and quantum mechanics (QM), we consider the one-lattice limit where the behavior of the ϕ^4 field theory resembles that of the PQHO. By numerically solving the eigenequations of the Hamiltonians, we obtain the ground states for both systems. The results, shown in Fig. 7, reveal good agreement in terms of the true values and trends for different coupling strengths between weak measurements in QFT and QM. However, it is worth noting that weak measurements in QFT, based on the quantum variation principle, exhibit less accuracy than the weak measurements in QM under the same conditions. This discrepancy arises due to the approximation $\delta p = p' - p$, which introduces uncertainty in variation δp. In the QFT context, this approximation may not hold as well, leading to less precise results in weak measurements compared to QM. Further investigation and analysis are necessary to understand the specific factors contributing to the differences between weak measurements in QFT and QM. By examining the limitations and approximations involved, we can gain insights into the nature of weak measurements in both frameworks.

[1] J. Schwinger, On the Green's functions of quantized fields. I, Proc. Natl. Acad. Sci. USA **37**, 452

(1951); On the Green's functions of quantized fields. II, **37**, 455 (1951).

[2] L. P. Kadanoff, *Quantum Statistical Mechanics* (CRC Press, Boca Raton, 2018).

[3] K. Hashimoto, K. Murata, and R. Yoshii, Out-of-time-order correlators in quantum mechanics, J. High Energy Phys. 10 (2017) 138.

[4] N. Yunger Halpern, Jarzynski-like equality for the out-of-time-ordered correlator, Phys. Rev. A **95**, 012120 (2017).

[5] T. Xu, T. Scaffidi, and X. Cao, Does scrambling equal chaos? Phys. Rev. Lett. **124**, 140602 (2020).

[6] Q. Bin, L.-L. Wan, F. Nori, Y. Wu, and X.-Y. Lü, Out-of-time-order correlation as a witness for topological phase transitions, Phys. Rev. B **107**, L020202 (2023).

[7] Y. Aharonov, D. Z. Albert, and L. Vaidman, How the result of a measurement of a component of the spin of a spin-1/2 particle can turn out to be 100, Phys. Rev. Lett. **60**, 1351 (1988).

[8] A. C. Elitzur and L. Vaidman, Quantum mechanical interaction-free measurements, Found. Phys. **23**, 987 (1993).

[9] Y. Aharonov, S. Popescu, D. Rohrlich, and P. Skrzypczyk, Quantum Cheshire Cats, New J. Phys. **15**, 113015 (2013).

[10] A. Danan, D. Farfurnik, S. Bar-Ad, and L. Vaidman, Asking photons where they have been, Phys. Rev. Lett. **111**, 240402 (2013)

[11] Y. Aharonov, E. Cohen, and A. C. Elitzur, Foundations and applications of weak quantum measurements, Phys. Rev. A **89**, 052105 (2014).

[12] E. Sjöqvist, Geometric phase in weak measurements, Phys. Lett. A **359**, 187 (2006).

[13] M. Cormann, M. Remy, B. Kolaric, and Y. Caudano, Revealing geometric phases in modular and weak values with a quantum eraser, Phys. Rev. A **93**, 042124 (2016).

[14] L. Li, Q.-W. Wang, S.-Q. Shen, and M. Li, Geometric measure of quantum discord with weak measurements, Quant. Inf. Process. **15**, 291 (2016).

[15] S. Wu, State tomography via weak measurements, Sci. Rep. **3**, 1193 (2013).

[16] L. Qin, L. Xu, W. Feng, and X.-Q. Li, Qubit state tomography in a superconducting circuit via weak measurements, New J. Phys. **19**, 033036 (2017).

[17] R. Uola, A. C. S. Costa, H. C. Nguyen, and O. Gühne, Quantum steering, Rev. Mod. Phys. **92**, 015001 (2020).

[18] S. Roy, J. T. Chalker, I. V. Gornyi, and Y. Gefen, Measurement-induced steering of quantum systems, Phys. Rev. Res. **2**, 033347 (2020).

[19] Y. Ding, Y. Pan, and X. Chen, Superoscillating quantum control induced by sequential selections, arXiv:2305.04303.

[20] Y. Pan, J. Zhang, E. Cohen, C.-W. Wu, P.-X. Chen, and N. Davidson, Weak-to-strong transition of quantum measurement in a trapped-ion system, Nat. Phys. **16**, 1206 (2020).

[21] V. Gebhart, K. Snizhko, T. Wellens, A. Buchleitner, A. Romito, and Y. Gefen, Topological transition in measurement-induced geometric phases, Proc. Natl. Acad. Sci. USA **117**, 5706 (2020).

[22] M. Gell-Mann and F. Low, Bound states in quantum field theory, Phys. Rev. **84**, 350 (1951).

[23] Y. Aharonov, P. G. Bergmann, and J. L. Lebowitz, Time symmetry in the quantum process of measurement, Phys. Rev. **134**, B1410 (1964).

[24] Y. Aharonov and L. Vaidman, The Two-State Vector Formalism: An Updated Review, in *Time in Quantum Mechanics*, edited by J. Muga, R. S. Mayato, and I. Egusquiza, Lecture Notes in Physics, Vol. 734 (Springer, Berlin, Heidelberg, 2018), pp. 399–477.

[25] T. Sagawa, Weak value and correlation function, arXiv:0901.4212.

[26] R. Jozsa, Complex weak values in quantum measurement, Phys. Rev. A **76**, 044103 (2007).

[27] J. Dressel, K. Y. Bliokh, and F. Nori, Classical field approach to quantum weak measurements, Phys. Rev. Lett. **112**, 110407 (2014).

[28] A. N. Korotkov, Selective quantum evolution of a qubit state due to continuous measurement, Phys. Rev. B **63**, 115403 (2001).

[29] K. Jacobs and D. A. Steck, A straightforward introduction to continuous quantum measurement, Contemp. Phys. **47**, 279 (2006).

[30] A. K. Pati, U. Singh, and U. Sinha, Measuring non-Hermitian operators via weak values, Phys. Rev. A **92**, 052120 (2015).

[31] K. A. Milton, *Schwinger's Quantum Action Principle* (Springer, Cham, 2015).

[32] A. Brodutch and L. Vaidman, Measurements of non local weak values, J. Phys.: Conf. Ser. **174**, 012004 (2009).

[33] K. J. Resch and A. M. Steinberg, Extracting joint weak values with local, single-particle measurements, Phys. Rev. Lett. **92**, 130402 (2004).

[34] V. Mnih, C. Szepesvári, and J. Y. Audibert, Empirical Bernstein stopping, in *Proceedings of the 25th International Conference on Machine Learning, Helsinki, 2008* (ACM, New York, 2008).

[35] H. Kleinert, *Particles and Quantum Fields* (World Scientific, Singapore, 2016).

[36] D. Guéry-Odelin, A. Ruschhaupt, A. Kiely, E. Torrontegui, S. Martínez-Garaot, and J. G. Muga, Shortcuts to adiabaticity: Concepts, methods, and applications, Rev. Mod. Phys. **91**, 045001 (2019).

[37] C. W. Duncan and A. del Campo, Shortcuts to adiabaticity assisted by counterdiabatic Born-Oppenheimer dynamics, New J. Phys. **20**, 085003 (2018).

[38] L. Lamata, J. León, T. Schätz, and E. Solano, Dirac equation and quantum relativistic effects in a single trapped ion, Phys. Rev. Lett. **98**, 253005 (2007).

[39] L. García-Álvarez, I. L. Egusquiza, L. Lamata, A. del Campo, J. Sonner, and E. Solano, Digital quantum simulation of minimal AdS/CFT, Phys. Rev. Lett. **119**, 040501 (2017).

[40] R. van Leeuwen, N. Dahlen, G. Stefanucci, C.-O. Almbladh, and U. von Barth, Introduction to the Keldysh Formalism, in *Time-Dependent Density Functional Theory*, edited by M. A. Marques, C. A. Ullrich, F. Nogueira, A. Rubio, K. Burke, and E. K. Gross, Lecture Notes in Physics, Vol. 706 (Springer, Berlin, Heidelberg, 2006), pp. 33–59.

[41] A. Cresti, R. Farchioni, G. Grosso, and G. P. Parravicini, Keldysh-Green function formalism for current profiles in mesoscopic systems, Phys. Rev. B **68**, 075306 (2003).

[42] A. Czajka and S. Mrówczyński, Ghosts in Keldysh-Schwinger formalism, Phys. Rev. D **89**, 085035 (2014).

[43] M. F. Maghrebi and A. V. Gorshkov, Nonequilibrium many-body steady states via Keldysh formalism, Phys. Rev. B **93**, 014307 (2016).

[44] https://github.com/GnefnAuy/GF-WV